



Connecting wall modes and boundary zonal flows in rotating Rayleigh-Bénard convection

Robert E. Ecke ^{1,2,3,*} Xuan Zhang ^{1,†} and Olga Shishkina ^{1,‡}

¹Max Planck Institute for Dynamics and Self-Organization, 37077 Göttingen, Germany

²Center for Nonlinear Studies, Los Alamos National Laboratory, Los Alamos, New Mexico 87545, USA

³Department of Physics, University of Washington, Seattle, Washington 98195, USA



(Received 17 June 2021; accepted 7 December 2021; published 10 January 2022)

Using direct numerical simulations, we study rotating Rayleigh-Bénard convection in a cylindrical cell with aspect ratio $\Gamma = 1/2$, for Prandtl number 0.8, Ekman number 10^{-6} , and Rayleigh numbers from the onset of wall modes to the geostrophic regime, an extremely important one in geophysical and astrophysical contexts. We connect linear wall-mode states that occur prior to the onset of bulk convection with the boundary zonal flow that coexists with turbulent bulk convection in the geostrophic regime through the continuity of length and timescales and of convective heat transport. We quantitatively collapse drift frequency, boundary length, and heat transport data from numerous sources over many orders of magnitude in Rayleigh and Ekman numbers. Elucidating the heat transport contributions of wall modes and of the boundary zonal flow are critical for characterizing the properties of the geostrophic regime of rotating convection in finite, physical containers and is crucial for connecting the geostrophic regime of laboratory convection with geophysical and astrophysical systems.

DOI: [10.1103/PhysRevFluids.7.L011501](https://doi.org/10.1103/PhysRevFluids.7.L011501)

Rayleigh-Bénard convection with rotation (RRBC) about a vertical axis is a prototypical laboratory realization of geophysical and astrophysical systems that combines buoyancy forcing and rotation [1–10]. Much recent experimental [8,11–14] and theoretical/numerical interest [15–17] on rotating convection has focused on the geostrophic regime where rotation dominates. In particular, one is interested in the scaling of local and global characteristics of the convecting state. An accessible and important global parameter is the normalized heat transport Nu for which there are theoretical predictions of asymptotic models [15–17] that provide insight into broader geo- and astrophysical situations. There are significant experimental challenges [18] for making a compelling comparison including reaching small Ek number with correspondingly large Ra. Consequently, the geometry of experimental convection cells have tended toward small aspect ratio $\Gamma = D/H < 1$, where D and H are the cell diameter and height, respectively. Recently several investigations [19–22] have revealed a boundary zonal flow (BZF) where an azimuthally-periodic, wall-localized flow coexists, on average, with a turbulent bulk mode (here we define the BZF as the wall-localized

*ecke@lanl.gov

†xuan.zhang@ds.mpg.de

‡Olga.Shishkina@ds.mpg.de

Published by the American Physical Society under the terms of the [Creative Commons Attribution 4.0 International](https://creativecommons.org/licenses/by/4.0/) license. Further distribution of this work must maintain attribution to the author(s) and the published article's title, journal citation, and DOI. Open access publication funded by the Max Planck Society.

state in the presence of *any* bulk mode when rotation dominates or influences the convective state) that contributes strongly to total heat transport. The BZF has features reminiscent of wall mode states in RRBC that arise from a linear instability at smaller critical Ra_w than Ra_c of the bulk mode and are characterized by an integer mode number (in periodic geometry), an anticyclonic precession frequency, and a homogeneous time-independent (in the precessing frame) state [4,7,23–26]. A recent numerical study [22] provided evidence that the BZF was the nonlinear remnant of wall modes. Here we establish unambiguously through direct numerical simulation (DNS) and comparison among disparate data sets for the drift frequency that characterizes the average angular precession frequency ω_d of the modal pattern in the rotating frame, the radial length scale δ_0 defined by the closest to the sidewall first zero crossing of the azimuthal velocity at the midplane, and the heat transport Nu , that there is a continuous evolution of the wall mode states into the BZF which coexists with the bulk convection modes. We also find that the wall mode contribution to the heat transport plays an important role in determining the scaling of Nu in the geostrophic regime, a crucial element in a proper comparison among experiment, DNS, and theory.

The dimensionless control parameters in RRBC are the Rayleigh number $Ra = \alpha g \Delta H^3 / (\kappa \nu)$, Prandtl number $Pr = \nu / \kappa$, Ekman number $Ek = \nu / (2\Omega H^2)$, and cell aspect ratio Γ where α is isobaric thermal expansion coefficient, ν kinematic viscosity, κ fluid thermal diffusivity, g acceleration of gravity, Ω angular rotation rate, and Δ the temperature difference between horizontal confining plates. The global response of the system is the normalized heat transport Nu , and the time and length scales of the wall modes and of the BZF are the normalized precession frequency $\omega_d = \omega / \Omega$ and radial localization length scale δ_0 / H . We present data for $Ek = 10^{-6}$, $Pr = 0.8$, $\Gamma = 1/2$, and $2 \times 10^7 \leq Ra \leq 5 \times 10^9$ that spans the wall mode onset at $Ra_w = 2.8 \times 10^7$ through the onset of bulk convection at $Ra_c \approx 9 \times 10^8$. We use our results on this system over wider ranges of Ek and Ra [19,20] with data from other experiments and DNS [4,5,7,13,21,22] to test our proposed power-law scalings.

The regimes of rotating convection in finite containers are wall-mode states at the lowest $Ra \geq Ra_w$, a transition at Ra_c to a bulk state of rotating convection [1] in which rotation dominates over buoyancy in geostrophic balance [27], a state with $Ra > Ra_g$ where rotation and buoyancy are of equal importance, and the buoyancy dominated state where rotation becomes unimportant at the highest $Ra > Ra_r$. The first instability from the no-convection base state is to wall modes with critical Rayleigh number $Ra_w \approx 31.8Ek^{-1} + 46.5Ek^{-2/3}$ [28].

To emphasize the role of these wall modes, we plot the boundaries of rotating convection regimes in Fig. 1 in a parameter space of Ra/Ra_w and Ek . The transition to bulk rotating convection would occur in an infinite system via linear instability at $Ra_c \approx (8.7-9.6Ek^{1/6})Ek^{-4/3}$ [1,29,30]. In the presence of sidewalls, however, the transition to a bulk convection state depends on Γ and on the nonlinear state of the wall modes because of the non-zero base state [4] with $Nu > 1$.

Whereas at modest $Ek \gtrsim 10^{-5}$ the onset of bulk convection $Ra_c/Ra_w \lesssim 10$, for smaller Ek there is an expanding and more nonlinear range of wall modes. For large enough Ra at fixed Ek , buoyancy dominates over rotation, and the transition to this regime for $Ek \lesssim 10^{-6}$ and $Pr < 1$ is identified empirically as $Ra_r \sim Ek^{-2}$ [10,13,20]. In the region $Ra_c < Ra < Ra_r$, a BZF has been identified in both experimental and numerical studies [13,19–21]. Near Ra_c , Nu rises rapidly [2,4,8,14,17] over a range $Ra_c < Ra_g = cRa_c$, $3 \lesssim c \lesssim 6$ before a transition region where Nu increases less rapidly with Ra , finally approaching the buoyancy dominated approximate scaling $Nu \sim Ra^{1/3}$ beginning at Ra_r . Given the paucity of data and the unknown influences of wall-mode contributions to the heat transport in most cases, the dependence of Ra_g on Ek is fairly uncertain and the line we draw in Fig. 1 is a suggestive one based on Refs. [4,14,17]. To understand experiments and DNS in realistic, confined convection cells, it is crucial to characterize the role of wall modes on the nonlinear evolution from no convection into the geostrophic regime and to connect the wall modes with the BZF that exists in the turbulent geostrophic regime [19,21,22]. That is our task here.

A qualitative understanding of the evolution of the state of rotating convection can be gained by considering instantaneous midplane horizontal cross sections of temperature fields and associated streamlines and corresponding vertical temperature fields at the sidewall boundary ($r = 0.98R$).

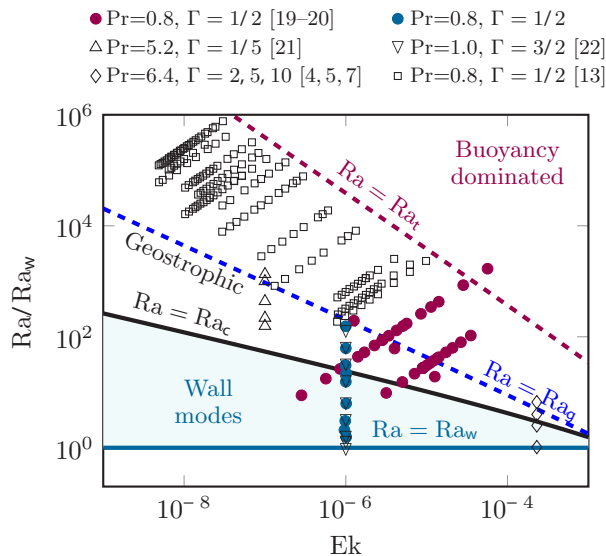


FIG. 1. Phase diagram of states of rotating Rayleigh–Bénard convection: Ra/R_{aw} vs Ek . Boundaries are for Ra_w , Ra_c , Ra_g , and R_a defined in the text.

Figure 2 shows these fields for several Ra [32]; also labeled is the reduced Ra defined as $\epsilon = Ra/R_{aw} - 1$ taking the experimental value $Ra_w = 2.8 \times 10^7$. Very close to onset ($\epsilon \approx 0.07$), the flow is organized as a mode-1 state with symmetric upwelling warmer (red) and downwelling cooler regions (blue), an overall anticyclonic rotation at the midplane, and a sinusoidal mean-temperature isotherm in the vertical field as shown in Fig. 2(a). The confined geometry of $\Gamma = 1/2$ means that the wall-mode temperature amplitude is not localised near the sidewall as in larger Γ [5,7] but has an almost linear variation across the diameter as in Fig. 2(a). Thus, when the bulk mode appears at higher Ra , it grows from a nonzero base state.

With increasing Ra , the wall-mode state becomes more nonlinear but time-independent (in a frame corotating with the retrograde traveling wall mode) for $Ra \lesssim 4 \times 10^8$. The state presented in Fig. 2(b) for $Ra = 5 \times 10^8$ shows the more complex horizontal temperature field and flow circulation and the strongly nonlinear square-wave-like vertical profile with forward/backward (left/right) asymmetry; it is also weakly time dependent indicating a wall-mode transition to an oscillatory state. For larger Ra , Fig. 2(c), the streamlines are irregular, indicating unsteady flow and thermal inhomogeneity appears in the interior. One sees vertical striations arising from the influence of aperiodic time-dependent bulk modes interacting with the wall mode.

The wall mode state is characterized by four main properties that we consider here: the heat transport Nu , the precession frequency ω , the azimuthal mode number, and the radial distribution of heat transport or azimuthal velocity u_ϕ . The azimuthal mode number is 1 because of small $\Gamma = 1/2$. Previously we demonstrated that for the BZF $m = 1$ for $\Gamma \leq 3/4$ and $m = 2\Gamma$ for $\Gamma = 1$ or 2 [20]. Our data show continuity from wall mode to BZF for this Γ .

We first consider the heat transport and its contributions from the wall mode, from the bulk state, and from the BZF. In Fig. 3(a), we show Nu versus Ra that covers the wall mode regime $3 \times 10^7 < Ra < 5 \times 10^8$, a transition region $5 \times 10^8 < Ra < 9 \times 10^9$, and the onset of strong bulk modes coexisting with remnant sidewall-localized modes, i.e., a BZF. The inset shows linear growth of the wall mode heat transport near onset consistent with the expected scaling $Nu - 1 = a\epsilon$ with $a \approx 1.54$ and $Ra_w = 2.8 \times 10^7$ (compared to the theoretical value 3.2×10^7 for an insulating sidewall and a planar (as opposed to a curved wall in cylindrical geometry) wall [25,32]). As the wall modes become more nonlinear, Nu increases less rapidly and approaches an inflection point around

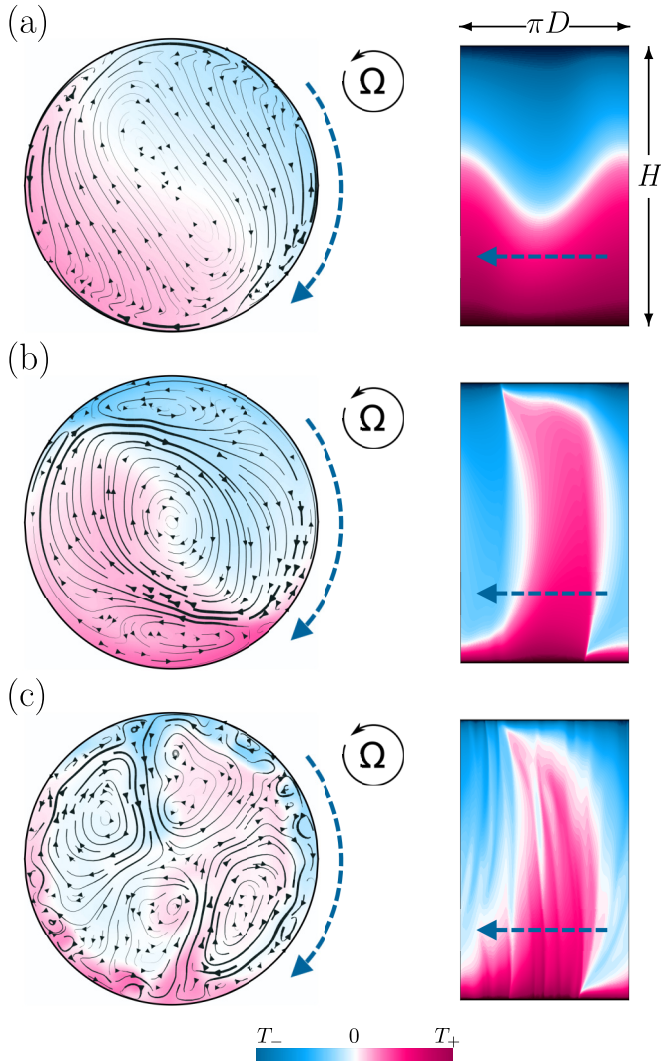


FIG. 2. Instantaneous temperature fields (left—horizontal at $z = H/2$ with streamlines; right—vertical at $r = 0.98R$) for $\text{Ek} = 10^{-6}$. Corresponding Ra and ϵ : (a) 3×10^7 , 0.071, (b) 5×10^8 , 17, (c) 1×10^9 , 35. Directions of rotation and wall mode precession are shown.

$\text{Ra} \approx 5 \times 10^8$ where a weak signature of time-dependent convection can be detected (vertical bars denote root-mean-square fluctuations). At slightly higher $\text{Ra} \approx 7 \times 10^8$, bulk modes begin to grow as demonstrated in instantaneous horizontal and vertical slices. At $\text{Ra} \approx 10^9$, Nu increases rapidly as bulk convection and wall localized convection act together. In Figs. 3(b) and 3(c), total Nu increases roughly linearly from an effective $\text{Nu}_{\text{off}} \approx 9$ and $\text{Ra}_c = 8.9 \times 10^8$ (compared to linear-stability prediction $\text{Ra}_c \approx 7.8 \times 10^8$ for $\text{Ek} = 10^{-6}$ [29]). Given the nonlinear base state created by the wall modes, the correspondence for the onset of bulk convection is good.

To further explore the relative contributions of the wall localized states and the bulk state, we divide up the heat transport according to a radial separation r_0 (normalized by cell radius R). We denote the portion from 0 to r_0 as contributing to the bulk state whereas the remaining portion from r_0 to 1 is attributed to wall states. In the language of Ref. [19], the wall portion is the nonlinear

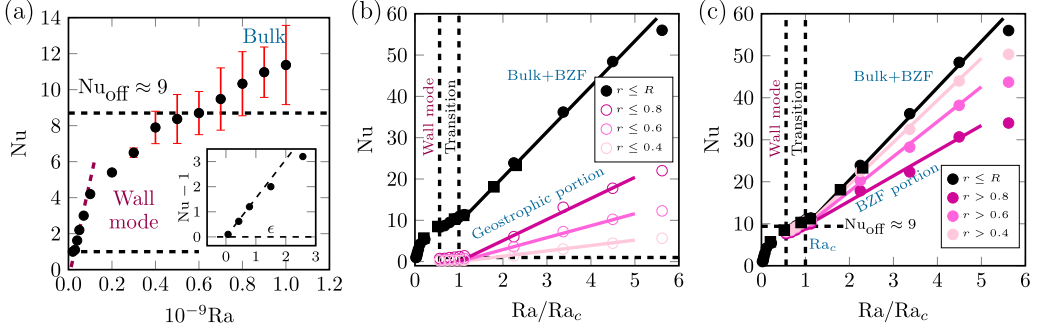


FIG. 3. Nu vs Ra for $\text{Pr} = 0.8$, $\text{Ek} = 10^{-6}$ and $\Gamma = 1/2$. (a) Time-dependent wall modes $\text{Ra} < 5 \times 10^8$ and onset of bulk convection for $\text{Ra} \gtrsim 9 \times 10^8$. Vertical bars are standard deviations of Nu fluctuations. Short-dashed line indicates linear fit to the data near onset (inset $\text{Nu} - 1$ vs ϵ near onset). Nu_{off} is the amount contributed by wall modes at bulk convection onset. [(b), (c)] Larger range of Ra with total Nu (solid, black) vs Ra/Ra_c and contributions averaged over regions defined by $r/R \leq r_0$ (bulk modes) and $r/R > r_0$ (wall modes/BZF). Black squares are the data from Ref. [20] for fixed $\text{Ra} = 10^9$. Solid lines are linear fits for $\text{Ra}/\text{Ra}_c \lesssim 5$.

BZF whereas the bulk convection is rotation dominated and in the geostrophic regime (similar decompositions [20,21] have demonstrated relative wall and bulk contributions to Nu in the BZF region). Although the quantitative split between different regions depends on the choice of r_0 , the trends are unambiguous. Both the BZF and bulk portions grow roughly linearly for $\text{Ra}/\text{Ra}_c \lesssim 5$. Nevertheless, the BZF remains larger throughout the range studied here. The bulk/geostrophic contribution to Nu over the range $\text{Ra}/\text{Ra}_c \lesssim 5$ is comparable to the asymptotic equation prediction for $\text{Pr} = 1$ [16] whereas the much larger total Nu is similar in magnitude to measurements in the same Ek range for $\Gamma = 0.4$ and $\text{Pr} = 4.4$ [14]; the contribution of wall-mode and BZF modes to the heat transport are important for comparisons with theoretical predictions.

We present in Figs. 4(a), 4(b) and 4(c), respectively, the Ra dependence of Nu, ω_d , and δ_0 in the wall mode region. We use $\epsilon = \text{Ra}/\text{Ra}_w - 1$ as the abscissa and plot the quantities $\text{Nu} - 1$, $\omega_d - \omega_{d_c}$ (inset shows expected linear ϵ dependence of ω_d), and $(\delta_0/H)\text{Ek}^{-2/3}$ (the factor $\text{Ek}^{-2/3}$ nicely collapses the data for $\text{Pr} = 0.8$ and $\text{Pr} = 6.4$ [4,5,7]), respectively. Here we use the asymptotic linear stability result for a planar wall [28] for the precession frequency at onset $\omega_{d_c} \approx (132 \text{Ek} - 1465 \text{Ek}^{4/3})\text{Pr}^{-1}$ [25,32]. The trends show the nonlinear evolution of the wall mode states with increasing Ra.

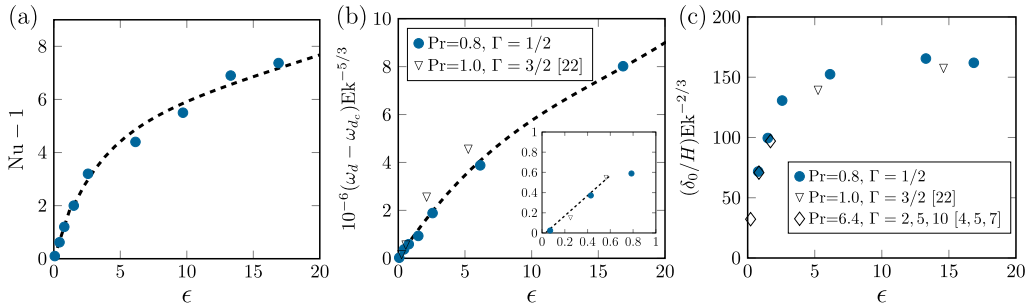


FIG. 4. (a) Nusselt number vs ϵ , (b) $(\omega_d - \omega_{d_c})\text{Ek}^{-5/3}$ (inset linear dependence on ϵ near onset), and (c) $(\delta_0/H)\text{Ek}^{-2/3}$ vs ϵ [31].

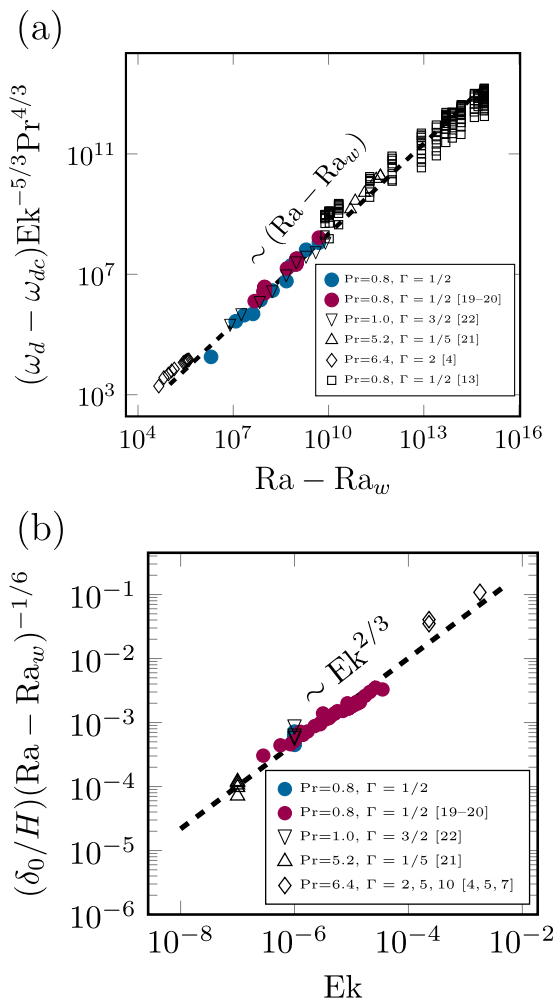


FIG. 5. Scaled (a) boundary mode drift frequency $(\omega_d - \omega_{dc}) \text{Ek}^{-5/3} \text{Pr}^{4/3} \approx 0.022(\text{Ra} - \text{Ra}_w)$ and (b) side-wall boundary length scale $(\delta_0/H)(\text{Ra} - \text{Ra}_w)^{-1/6} \approx 1.0 \text{Ek}^{2/3}$.

We now show trends in ω_d and δ_0 extending over many decades in Ra and Ek that spans the wall mode region and the geostrophic region coexisting with the BZF using data from our previous simulations on this system [19,20] as well as from others for which these quantities have been measured [4,13,21,22]. In Figs. 5(a) and 5(b) we show scaled quantities $(\omega_d - \omega_{dc}) \text{Ek}^{-5/3} \text{Pr}^{4/3} \approx 0.022(\text{Ra} - \text{Ra}_w)$ (consistent with [20]) and $(\delta_0/H)(\text{Ra} - \text{Ra}_w)^{-1/6} \approx 4.7 \text{Ek}^{2/3}$ (the data for $\text{Ek} = 10^{-6}$ are consistent with the scalings determined by us elsewhere [19,20] and with other data [4,5,7,13,21,22]). The Ra and ω_d dependences are corrected for their finite values at the onset of wall modes using $\text{Ra} - \text{Ra}_w$ and $\omega_d - \omega_{dc}$, respectively. The collapse over almost 10 decades in $\text{Ra} - \text{Ra}_w$ [Fig. 5(a)] showing $\omega_d - \omega_{dc} \sim \text{Ra} - \text{Ra}_w$ and over 4 decades in Ek showing $\delta_0 \sim \text{Ek}^{2/3}$, see Fig. 5(b), establishes the connection between the wall modes and the BZF.

In conclusion, we have demonstrated the continuity of measures of time, length, and heat transport from the wall mode state through the appearance of bulk modes coexisting with the BZF, unambiguously connecting the two states. We show that by accounting for the wall mode contribution Nu_{off} and by considering the radial distribution of Nu (see also Ref. [21]), the bulk Nu in the geostrophic regime can be extracted with a scaling consistent with a linear dependence

for $Ra/Ra_c \lesssim 5$. Our analysis of Nu data accounting for the wall-mode/BZF contributions seems essential in considering the Nu scaling of rotating convection in the rapidly rotating regime for finite geometries.

The authors acknowledge support from the Deutsche Forschungsgemeinschaft (DFG), SPP 1881 “Turbulent Superstructures” and Grants No. Sh405/7 and No. Sh405/8, from the LDRD program at Los Alamos National Laboratory and by the Leibniz Supercomputing Centre (LRZ).

-
- [1] S. Chandrasekhar, *Hydrodynamic and Hydromagnetic Stability* (Clarendon Press, Oxford, UK, 1961).
 - [2] T. H. Rossby, A study of Bénard convection with and without rotation, *J. Fluid Mech.* **36**, 309 (1969).
 - [3] J. M. Pfothenauer, P. G. J. Lucas, and R. J. Donnelly, Stability and heat transfer of rotating cryogenics. Part 2. Effects of rotation on heat-transfer properties of convection in liquid ^4He , *J. Fluid Mech.* **145**, 239 (1984).
 - [4] F. Zhong, R. Ecke, and V. Steinberg, Rotating Rayleigh–Bénard convection: Asymmetric modes and vortex states, *J. Fluid Mech.* **249**, 135 (1993).
 - [5] L. Ning and R. E. Ecke, Rotating Rayleigh–Bénard convection: Aspect-ratio dependence of the initial bifurcations, *Phys. Rev. E* **47**, 3326 (1993).
 - [6] K. Julien, S. Legg, J. McWilliams, and J. Werne, Rapidly rotating turbulent Rayleigh–Bénard convection, *J. Fluid Mech.* **322**, 243 (1996).
 - [7] Y. Liu and R. E. Ecke, Nonlinear traveling waves in rotating Rayleigh–Bénard convection: Stability boundaries and phase diffusion, *Phys. Rev. E* **59**, 4091 (1999).
 - [8] E. M. King, S. Stellmach, J. Noir, U. Hansen, and J. M. Aurnou, Boundary layer control of rotating convection systems, *Nature (London)* **457**, 301 (2009).
 - [9] J.-Q. Zhong, R. J. A. M. Stevens, H. J. H. Clercx, R. Verzicco, D. Lohse, and G. Ahlers, Prandtl-, Rayleigh-, and Rossby-Number Dependence of Heat Transport in Turbulent Rotating Rayleigh–Bénard Convection, *Phys. Rev. Lett.* **102**, 044502 (2009).
 - [10] R. Kunnen, The geostrophic regime of rapidly rotating turbulent convection, *J. Turbulence* **22**, 267 (2021).
 - [11] R. E. Ecke and J. J. Niemela, Heat Transport in the Geostrophic Regime of Rotating Rayleigh–Bénard Convection, *Phys. Rev. Lett.* **113**, 114301 (2014).
 - [12] J. S. Cheng, M. Madonia, A. J. Aguirre Guzmán, and R. P. J. Kunnen, Laboratory exploration of heat transfer regimes in rapidly rotating turbulent convection, *Phys. Rev. Fluids* **5**, 113501 (2020).
 - [13] M. Wedi, D. V. Gils, E. Bodenschatz, and S. Weiss, Rotating turbulent thermal convection at very large Rayleigh numbers, *J. Fluid Mech.* **912**, A30 (2021).
 - [14] H.-Y. Lu, G.-Y. Ding, J.-Q. Shi, K.-Q. Xia, and J.-Q. Zhong, Heat-transport scaling and transition in geostrophic rotating convection with varying aspect ratio, *Phys. Rev. Fluids* **6**, L071501 (2021).
 - [15] M. Sprague, K. Julien, E. Knobloch, and J. Werne, Numerical simulation of an asymptotically reduced system for rotationally constrained convection, *J. Fluid Mech.* **551**, 141 (2006).
 - [16] K. Julien, E. Knobloch, A. M. Rubio, and G. M. Vasil, Heat Transport in Low-Rossby-Number Rayleigh–Bénard Convection, *Phys. Rev. Lett.* **109**, 254503 (2012).
 - [17] S. Stellmach, M. Lischper, K. Julien, G. Vasil, J. S. Cheng, A. Ribeiro, E. M. King, and J. M. Aurnou, Approaching the Asymptotic Regime of Rapidly Rotating Convection: Boundary Layers Versus Interior Dynamics, *Phys. Rev. Lett.* **113**, 254501 (2014).
 - [18] J. S. Cheng, J. M. Aurnou, K. Julien, and R. P. J. Kunnen, A heuristic framework for next-generation models of geostrophic convective turbulence, *Geophys. Astrophys. Fluid Dyn.* **112**, 277 (2018).
 - [19] X. Zhang, D. P. M. van Gils, S. Horn, M. Wedi, L. Zwirner, G. Ahlers, R. E. Ecke, S. Weiss, E. Bodenschatz, and O. Shishkina, Boundary Zonal Flow in Rotating Turbulent Rayleigh–Bénard Convection, *Phys. Rev. Lett.* **124**, 084505 (2020).
 - [20] X. Zhang, R. E. Ecke, and O. Shishkina, Boundary zonal flows in rapidly rotating turbulent Rayleigh–Bénard convection, *J. Fluid Mech.* **915**, A62 (2021).

- [21] X. M. de Wit, A. J. Aguirre Guzman, M. Madonia, J. S. Cheng, H. J. H. Clercx, and R. P. J. Kunnen, Turbulent rotating convection confined in a slender cylinder: The sidewall circulation, *Phys. Rev. Fluids* **5**, 023502 (2020).
- [22] B. Favier and E. Knobloch, Robust wall states in rapidly rotating Rayleigh–Bénard convection, *J. Fluid Mech.* **895**, R1 (2020).
- [23] F. Zhong, R. Ecke, and V. Steinberg, Asymmetric Modes and the Transition to Vortex Structures in Rotating Rayleigh–Bénard Convection, *Phys. Rev. Lett.* **67**, 2473 (1991).
- [24] H. F. Goldstein, E. Knobloch, I. Mercader, and M. Net, Convection in a rotating cylinder. Part 1 Linear theory for moderate Prandtl numbers, *J. Fluid Mech.* **248**, 583 (1993).
- [25] J. Herrmann and F. H. Busse, Asymptotic theory of wall-attached convection in a rotating fluid layer, *J. Fluid Mech.* **255**, 183 (1993).
- [26] E. Y. Kuo and M. C. Cross, Traveling-wave wall states in rotating Rayleigh–Bénard convection, *Phys. Rev. E* **47**, R2245(R) (1993).
- [27] K. Julien, A. M. Rubio, I. Grooms, and E. Knobloch, Statistical and physical balances in low Rossby number Rayleigh–Bénard convection, *Geophys. Astrophys. Fluid Dyn.* **106**, 392 (2012).
- [28] The first term computed for free-slip horizontal boundaries and $\text{Ek} \rightarrow 0$ [25] was extended to include a second term which is the first-order finite Ek correction for realistic no-slip conditions [33].
- [29] P. P. Niiler and F. E. Bisshopp, On the influence of Coriolis force on onset of thermal convection, *J. Fluid Mech.* **22**, 753 (1965).
- [30] G. M. Homsy and J. L. Hudson, The asymptotic stability of a bounded rotating fluid heated from below: Conductive basic state, *J. Fluid Mech.* **45**, 353 (1971).
- [31] The δ_0 data using the zero-crossing of u_ϕ for $\text{Pr} = 1$, $\Gamma = 3/2$, and $\text{Ek} = 10^{-6}$ [22] are depth averaged whereas our results are obtained at the midplane. To compensate this difference we compute the difference for midplane and depth-averaged in our simulations versus Γ and apply the resulting correction factor 1.3 to the results in Ref. [22] and 1.4 to the results in Refs. [4,5,7]. The data for $\text{Pr} = 6.4$ are obtained from shadowgraph images (related to the thermal field as opposed to the azimuthal velocity field) corresponding to values near the transition to bulk convection for different conditions: $\{\Gamma, \text{Ek}, \epsilon\}$: 2, 2.3×10^{-4} , 0.84 [4]; 5, 2.3×10^{-4} , 1.7 [5]; 10, 1.8×10^{-3} , 0.22 [7].
- [32] See Supplemental Material at <http://link.aps.org/supplemental/10.1103/PhysRevFluids.7.L011501> for evolution of the temperature field for the cases in Fig. 2.
- [33] K. Zhang and X. Liao, The onset of convection in rotating circular cylinders with experimental boundary conditions, *J. Fluid Mech.* **622**, 63 (2009).